Desalination and Water Treatment
www.deswater.com
doi: 10.1080/19443994.2014.972466

57 (2016) 505–517
January

Taylor & Francis
Taylor & Francis Group

System dynamics modeling and simulation of a coagulation–ultrafiltration process for the treatment of drinking water

Yueqi Zhu[a,*], Xuehua Zhang[b], Hongwei Zhang[a]

[a]*Department of Environmental Science and Engineering, Tianjin University, Tianjin 300072, China, Tel. +86 13821653658; Fax: +86 022 23121662; email: hunanzhilv@163.com (Y. Zhu), Tel. +86 13502171853; email: hwzhang@tju.edu.cn (H. Zhang)*
[b]*Department of Economics, Tianjin Polytechnic University, Tianjin 300050, China, Tel. +86 13920295002; email: xuehua671231@163.com (X. Zhang)*

Received 30 January 2014; Accepted 25 September 2014

ABSTRACT

In this work, a system dynamics (SD) model of a coagulation–ultrafiltration (UF) process was developed using Vensim and validated with experimental data. The SD model includes the basic elements and essential structure of the coagulation–UF process system. Numerical simulations were used to optimize the operating parameters of the SD model. The simulation results demonstrated that the absorption resistance (R_a) contributed a small portion of the total resistance (R_t) (≤15%) in the basic experiment, where the initial permeate flux (J_0) was 35 $m^3/(m^2\ h)$. Furthermore, the cake layer resistance (R_c) was the main cause of the total resistance (R_t) within the model. The concentration of coagulant and the removal rate of membrane fouling were positively correlated when the coagulant concentration increased from 20 to 35 mg/L. In addition, the contribution of total resistance to membrane fouling was obtained from the SD model. The membrane fouling rate reached 22.5 Pa/h after 16 backwashing cycles which corresponds to the predicted chemical cleaning time. The SD model presented here can provide guidance in optimizing operating parameters through numerical simulations which eschew the need for large amounts of repeated tests.

Keywords: System dynamics modeling; Coagulation–ultrafiltration process; Cake layer resistance; Membrane fouling; Drinking water treatment

1. Introduction

Membrane fouling is one of the serious problems that hinders extended utilization of membrane filtration processes [1]. Pretreatment, such as coagulation in front of the membranes, has been used to mitigate fouling. The effects of coagulation on membrane fouling have been extensively reported [2–4]. Previous studies focused on the operating parameters, which were tested by large numbers of experiments spanning various mixing conditions and coagulant doses. A number of researchers have studied, and identified the significant impacts of coagulation on fouling mitigation by using general water quality parameters to investigate the performance of each step in the treatment process. Barbot et al. found that coagulation reduced fouling by decreasing cake resistance, limiting pore blockage, and increasing backwash efficiency by jar test [5]. Staaks et al. evaluated coagulation efficiency with continuous monitoring of formation and breakage of flocs using a photometric

*Corresponding author.

dispersion analyzer (PDA) [6]. While these experiments were performed to investigate the effect of one factor or components of operating parameters on the membrane fouling removal computational approaches can be valuable in terms of understanding the system and evaluating its performance in a wider range of scenarios.

Traditionally, analytical methods have focused primarily on specific technical aspects [7,8]. For instance, there are a number of studies examining theoretical and semi-empirical models which were used in the study of fouling phenomena in the membrane processes [9]. Additionally, cake filtration theory was used to interpret data and calculate fouling resistances [10]. These methods present only static models of the membrane fouling system, lacking both the interactions between system components and feedback effects. Therefore, it is insufficient to thoroughly analyze the dynamic complexity of the coagulation–ultrafiltration (UF) process system, because the time-varying dynamic behavior of the coagulation–UF process has not been sufficiently elucidated.

System dynamics (SD) is a means for analyzing systems [11,12]. An SD model incorporates the key feedback structures in the system. Simulating the model shows the effect of the parameters optimization on system structure. This approach has been applied to a number of studies related to economics, environmental management, and social systems [13,14]. However, there have been no prior studies on SD simulation of coagulation–UF processes. Therefore, although such computer-based simulation tools are often used to help decision-makers to evaluate economics and management options, their potential for analyzing the treatment of drinking water could be further exploited. In particular, SD models enable study of the structure of the system and the overall coagulation–UF process with minimum technical experiments. In drinking water treatment units, the SD models can be used to investigate the performance of coagulation–UF process system under different dynamic scenarios.

In this paper, SD methodology was used to improve both the basic parameters and the operational instructions. In the SD model, changes in the resistance properties of coagulation–UF process system were investigated under various conditions along with their influence on membrane filtration and fouling. Different coagulation–UF process scenarios were simulated using varying parameters to explore a range of experimental conditions. Model performance was compared against experimental data from a waterworks reservoir. The effect of the coagulation on the membrane UF performance was evaluated by simulations incorporating varying concentrations of coagulant. The effect of the permeate flux on the membrane fouling length was also analyzed. The SD model showed the effects of backwashing, and time of chemical cleaning was predicted. Ultimately, this represents a new and practical approach toward the analysis of the dynamics of water treatment, because the SD model can be used to efficiently identify optimal operating parameters through numerical simulations, avoiding extensive experimental testing. Our model may also facilitate future work on the development of control strategies and operability.

2. Materials and methods

2.1. Experimental materials

The raw water in this study came from the influent stream of a waterworks reservoir (JZZ waterworks, Tianjin, China), sourced from the surfacewater of Luanhe River lying to the south of Tianjin City in China. The main pollutants in the raw water are natural organic matters. The raw water quality during the experiment is presented in Table 1.

All experiments were performed at room temperature, 25 ± 2°C. Ferric chloride (FeCl3; J&K Scientific Ltd, ACS) was used as coagulant to pretreat before filtration. Guigui et al. reported that coagulation with $FeCl_3$ significantly decreased the cake layer resistance (R_c) [15].

To optimize the mixing time of coagulation process, a PDA (PDA2000; Calibre (Beijing) Technology Development Co., Ltd; China) was used for realtime monitoring to determine floc size variance during flocculation [16,17]. This technique shows the change and the level of flocculation of suspended particulates by detecting fluctuations in transmitted light intensity. The relative fluctuation (R) correlates the diameter with the density of grains.

The relative fluctuation (R) was used to characterize the variance of the average particle size of flocs. As the rapid mixing time increased, R (−) increased, representing the period of flocs growth. However, the flocs broke into small sizes when the rapid mixing time was too long. On the other hand, as the slow mixing time increased, the R (−) decreased. In this regime, the flocs settled and the water became clear. When the R (−) remained constant, most flocs settled at the bottom of the container. In this test, the PDA was used to measure the optimum coagulation mixing time of coagulation. Fig. 1 schematically depicts the setup for conducting the jar test. In this way, turbidity was continuously monitored.

Table 1
Water quality parameters in the raw water

Water quality parameter	Measured values during the tests (2013)
Temperature, ℃	19.5–20.7
pH	7.98–8.43
Turbidity, NTU	6.34–10.90
$COD_{Mn,}$ mg/L	4.15–6.25
TOC, mg/L	5.45–7.21
$UV_{254,}$ cm^{-1}	0.030–0.066
NH_3-N, mg/L	0.05–0.09
Chlorophyll, mg/L	3.83–6.49
Algae, million/L	142–235

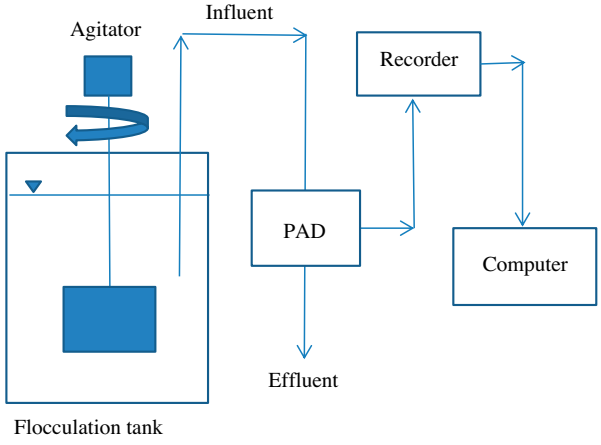

Fig. 1. Schematic diagram of the PDA setup.

The PDA was used in the experiment with different mixing speeds. Fig. 2 presents the changes in the relative fluctuation (R) under rapid mixing at 200 rpm for 240 s (4 min). The result indicates that the maximum value $R\ (-)_{max}$ occurred at 180 s (3 min). Then, equivalent slow mixing experiments were calculated. Fig. 3 presents the changes in the relative fluctuation (R) under slow mixing at 40 rpm for 30 min after the rapid mixing at 200 rpm for 180 s (3 min). This revealed that the minimum value of $R\ (-)_{min}$ occurred after 20 min, suggesting 20 min is enough for precipitation reaction (Fig. 3). Thus, $FeCl_3$ was added in the raw water and agitated for 23 min (rapid mixing of 3 min at 200 rpm and slow mixing of 20 min at 40 rpm). After that, the coagulated water was then allowed to settle for 30 min.

The supernatant was filtrated through hollow fiber membranes. Polyvinylidene fluoride UF hollow fiber membrane with a molecular weight cut-off of 150 kDa served as the membrane module. The membrane area was 0.04 m^2. MOTIANMO Corporation provided the membrane. The schematic diagram of the UF hollow fiber membrane module setup used in this study is shown in Fig. 4.

During the filtration phase, the flushing operation was conducted for 10 s by opening the feed and flushing valves for startup. The feed and permeate valves were opened to allow the feedwater to be filtrated for 100 min. After filtration was complete, 5 min of backwashing was performed by opening the backwashing valve. The pressures of filtration and backwashing were 0.1 MPa and 0.15 MPa, respectively. A new membrane module was used in each experiment.

One of the key issues in membrane technology is to avoid fouling formed on membrane surfaces [18]. Membrane fouling induces an increase in the transmembrane pressure (TMP), thus raises the operation costs of the plant. Therefore, backwashing is normally

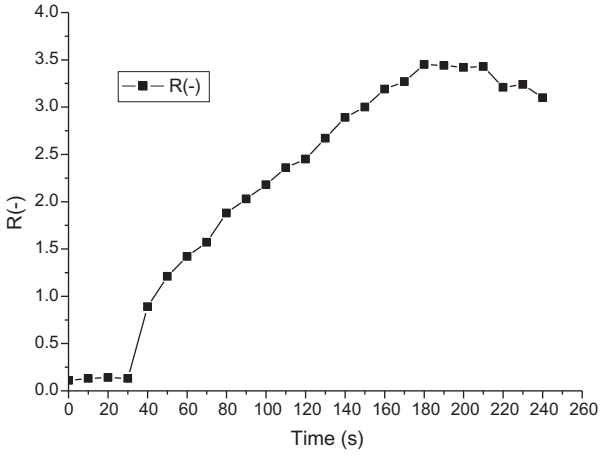

Fig. 2. Variation in R (−) value with rapid mixing.

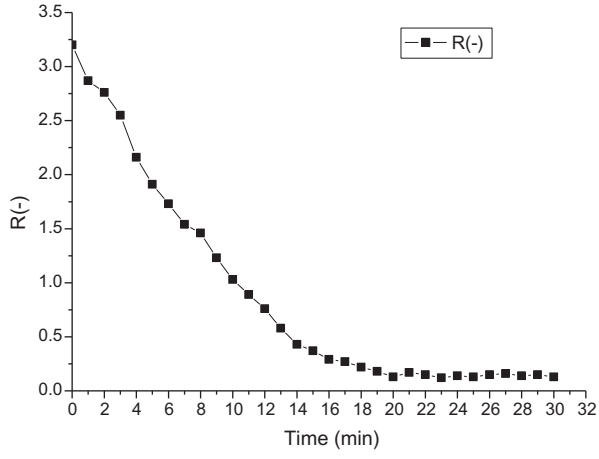

Fig. 3. Variation in R (−) value with low mixing.

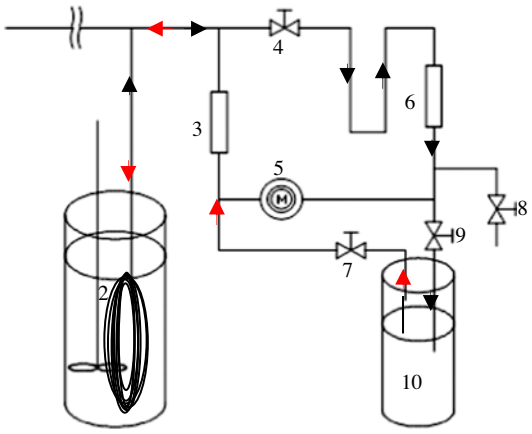

Fig. 4. Experimental setup: (1) mixer and reactor; (2) membrane module; (3) backwashing flowmeter; (4) feedwater valve; (5) pump; (6) permeate flowmeter; (7) backwashing water valve; (8) flushing valve; (9) permeate valve; and (10) circulating water tank.

suggested as a physical approach to reduce reversible fouling on the membrane surface. Along with this consideration, the TMPs were measured to calculate membrane resistances which describe the degree of fouling.

2.2. System dynamics

2.2.1. Elements of coagulation–UF process system model

Based on the fundamental systems premise that a system's structure generates its behavior, the first step in the development of a model of filtration and backwashing in the coagulation–UF process was to define the core elements of the system [19]. The filtration side of the system consists of temperature, flux, coagulant concentration, etc. The backwashing side of the system focuses on membrane fouling velocity, backwashing pressure, backwashing rate, and other factors. Table 2 shows the elements affecting filtration and backwashing and their connections.

2.2.2. Causal loop diagram

The dynamic hypothesis of our model can be conceptualized as a set of stocks and information flows. A causal loop diagram [20], shown in Fig. 5, was developed by incorporating the various features in Table 2 associated with the coagulation–UF process. The dynamics of the model were determined based on the feedback loops of the causal loop diagram. Each arrow of the causal loop diagram indicates the influence of

Table 2
Elements definitions of coagulation–UF process system model

Name of element	Definition
Adsorption resistance	Resistance of pore adsorption, m^{-1}
Backwashing flux	Backwashing flux passing through a unit membrane area in unit time, $m^3/(m^2\ h)$
Backwashing rate	Ratio of back washing time and membrane filtration time, %
Backwashing capacity	Water used for backwashing, m^3
Cake layer resistance	Resistance of cake layer, m^{-1}
Fiber length	Length of membrane fiber, cm
Filtering capacity	Filtrated water, m^3
Flux declining rate	Ratio of pure water flux after filtration and pure water membrane specific flux, %
Flux recovering rate	Ratio of pure water flux after backwashing and pure water membrane specific flux, %
Inside/outside diameter	The inside/outside diameter of membrane fiber, mm
Membrane fouling length	The length of the fouled membrane, cm
Membrane fouling rate	TMP in unit time, Pa/h
membrane resistance	Resistance by itself, m^{-1}
Net flux	Difference between permeate flux and backwashing flux, $m^3/(m^2\ h)$
Permeate flux	Flux of feed water, $m^3/(m^2\ h)$
Pure water membrane specific flux	The pure water flux of membrane, $L/(0.01\ Mpa\ m^2\ h)$
Temperature	Room temperature, ℃
TMP after backwashing	TMP of backwashing period, kPa
Transmembrane pressure	TMP of filtration period, kPa
Viscosity	Viscosity factor of feed water, Pa s

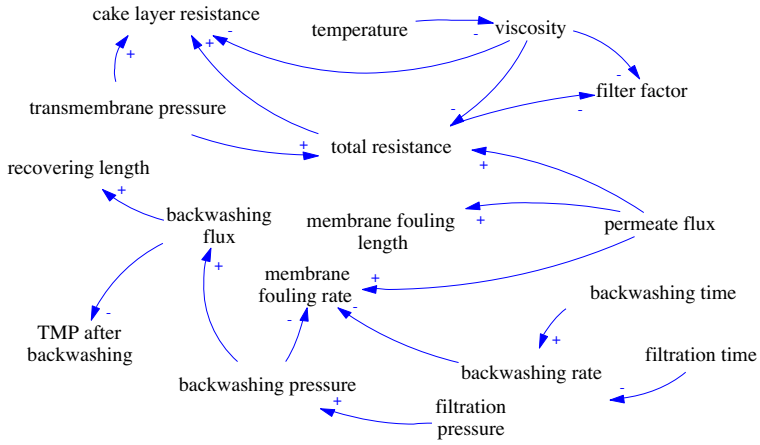

Fig. 5. Causal loop diagram of coagulation–UF process SD model ("+" on the arrow connecting two variables indicates the variable at the tail of the arrow causes a change in the variable at the head of the arrow in the same direction. "−" indicates a change in the opposite direction).

one element on the other, either positive (+) or negative (−) feedback.

2.2.3. Flow diagram

In the SD model, simulation progresses in sequential discrete time steps within a predefined time interval [21]. The model was implemented using Vensim PLE version 3.0 software [22]. A flow diagram was created from the causal loop diagram, and Vensim equations for each element in the diagram were added to the model. The model was run for a period of 105 min starting at 0 min. Fig. 6 shows the physical and information flows in the SD model.

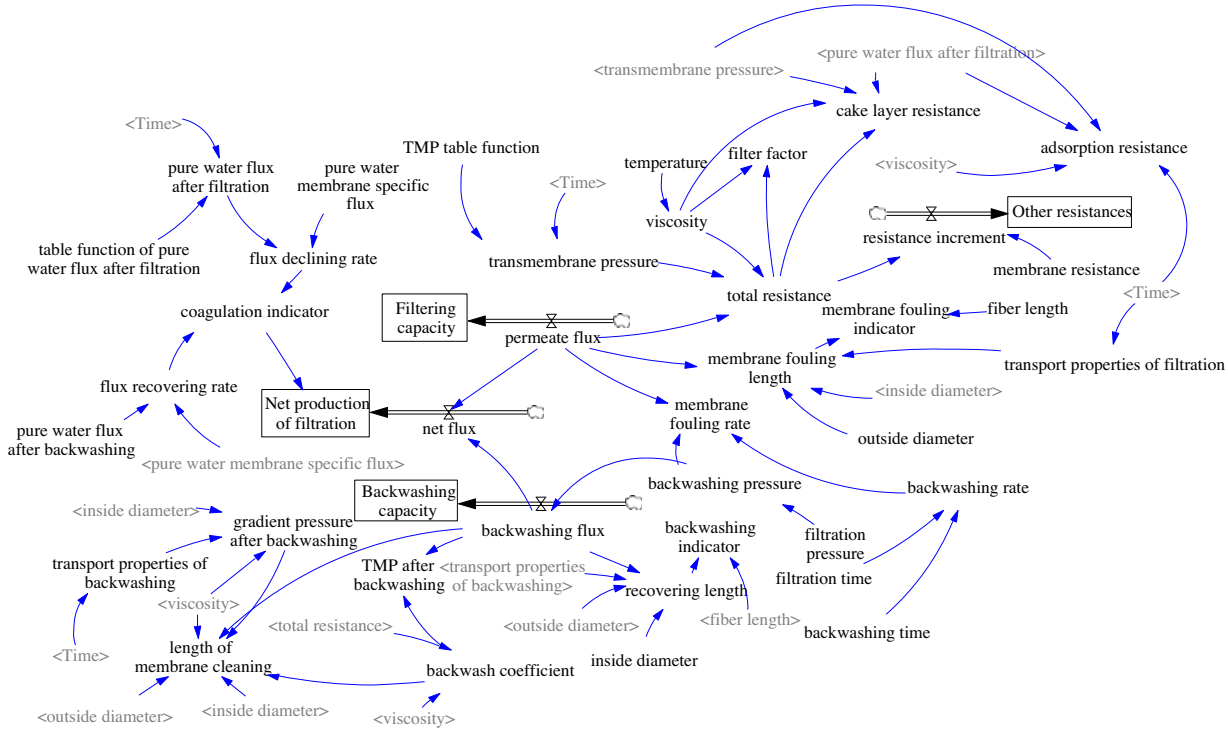

Fig. 6. Flow diagram of coagulation–UF process system SD model. (Boxes represent stocks, or accumulations in the system. Double arrows represent material flows, which are regulated by rate variables.)

The level variable (membrane flux production) is shown as a rectangular box, representing accumulated flows to that level. The rate variables (membrane flux and backwashing flux) are represented by valves. A double arrow represents physical flow, which is controlled by a flow rate. A single arrow shows connections and directionalities between variables. The sources and sinks of the structure are represented using a cloud, which indicates infinity and marks the boundary of the model.

Based on our experimental data, the Vensim equations used to account for variables in coagulation–UF process system are shown in Table 3.

2.2.4. Assumptions in the model

The causal relationships among variables, as shown in Fig. 6, are represented as equations in Vensim, thus forming a complete simulation model. The user can analyze and investigate the effects of perturbations to the model, both in terms of model structure and in the values of parameters and initial conditions.

The conditions of coagulation–UF process may vary over time and in response to external stimuli, and these changes propagate through to other components of the system. In this model, which is calibrated on our experimental data, the Vensim equations are used to interactively operate variables in the coagulation–UF process system.

The model boundary includes the original source of raw water supply and backwashing water supply, the supernatant, and the permeate water. It also includes the membrane module specification. Fig. 5 shows the major variables affecting filtration and backwashing and their connections. The feedback loop represents the coagulation–UF process mechanism. When TMP increases, total resistance rises. Meanwhile, increasing backwashing flux leads to an increase in the recovering length.

The model contains several simplifying assumptions. For instance, it assumes that the quality of raw water will remain stable during the experiment, the mechanism of the SD model is consistent with the coagulation–UF process, and the membrane module specification will remain unchanged. The model assumes that the most significant factor affecting the total resistance is cake layer resistance. The model also does not account for irreversible resistance and chemical cleaning. This assumption is valid throughout the filtration and backwashing processes. Resistance growth was projected based on Darcy's law [23]. Once the simulation is over, from 0 to 105 min (100 min of filtration and 5 min of backwashing), system variables are brought up to date, representing the results of a complete cycle, i.e. filtration, fouling, and backwashing. The flow diagram shows details of system variables, which vary as the simulation progresses.

3. Results and discussion

3.1. Build confidence in the model

Before using the model to analyze any coagulation–UF process system, it must be validated against experimental data. If the model successfully reproduces realistic trends and dynamics, we assume that the model contains the critical elements generating the experimental data.

The model-based output for the flux declining rate (Fig. 7) can be derived from the base model output in this study. The model projection curve is similar to the experimental data curve, confirming the fidelity of the proposed SD model. The prediction accuracy of flux declining rate from 0 to 100 min was further validated based on the extremely high R^2 value (0.9935). The model indicates that the pattern of the decline in the flux rate is driven by the water flux after filtration and the membrane specific flux.

To illustrate the characteristics of membrane filtration in the SD model, the permeate flux TMP was monitored at a constant flux (35 $m^3/(m^2\ h)$). A comparison of the experimental TMP data to the model projection was conducted and is shown in Fig. 8. The model reproduced the general trends of the TMP from 15.7 to 32.2 kPa. Experimental TMP ranged from approximately 17.8 to 36 kPa. As shown in Fig. 8, the difference between the experimental data and the model projection was minimal. This indicates that the model captures the essential structure of the system and can be used for further analysis. This was similar to the results obtained by Jang et al. [24]. They found that since the peristaltic pump driving out the permeate water did not change, the TMP increased naturally due to fouling, resulting in a decrease in the effective area of the membrane.

3.2. Analysis of coagulation–UF process SD model

3.2.1. Impact of the cake layer resistance and the adsorption resistance

The value of TMP over time was used to analyze resistance to membrane fouling. Based on our model, the permeate flux on the applied TMP can be described by Darcy's law, as follows [23]:

Table 3
Vensim equations derived in support of the SD model

Factors	Vensim equations
Adsorption resistance	(Transmembrane pressure/viscosity) × (1/pure water flux after filtration)/((Time)+1)
Backwashing flux	0 + STEP (backwashing pressure/35, 100)
Backwashing indicator	IF THEN ELSE(recovering length ≤ (1/3·fiber length), 1, 0)
Backwashing pressure	Filtration pressure × 5 × 100
Backwashing rate	Backwashing time/filtration time × 100
Backwashing time	5
Backwashing capacity	INTEG (backwashing flux, 0)
Cake layer resistance	Total resistance − (transmembrane pressure/viscosity/pure water flux after filtration)
Coagulation indicator	IF THEN ELSE((flux declining rate + (flux recovering rate − 0.5)) > 0, 1, 0)
Fiber length	40
Filter factor	1/(total resistance × viscosity)
Filtering capacity	INTEG (permeate flux, 0)
Filtration pressure	1
Filtration time	100
Flux declining rate	Pure water flux after filtration/pure water membrane specific flux
Flux recovering rate	0 + STEP(pure water flux after backwashing/pure water membrane specific flux, 100)
Gradient pressure after backwashing	Transport properties of backwashing × viscosity/inside diameter^2
Inside diameter	0.6
Length of membrane cleaning membrane fouling indicator	Backwashing flux × inside diameter^2 × gradient pressure after backwashing/(128 × viscosity·outside diameter + backwash coefficient)
Membrane fouling length	IF THEN ELSE(membrane fouling length ≤ fiber length, 1, 0)
Membrane fouling rate	4 × outside diameter × permeate flux × transport properties of filtration/inside diameter^2
Membrane resistance	8.36619 − 0.19052 × permeate flux − 0.045969 × backwashing pressure − 0.67579 × backwashing rate − 0.000532 × permeate flux × backwashing pressure + 0.004788 × permeate flux × backwashing rate + 0.000623333 × backwashing pressure × backwashing rate + 0.0038284 × permeate flux^2 + 0.000195122 × backwashing pressure^2 + 0.050678 × backwashing rate^2
Net flux	9.77e + 008

(*Continued*)

Table 3 (*Continued*)

Factors	Vensim equations
Net production of filtration	Permeate flux − backwashing flux
Other resistances	INTEG (net flux × coagulation indicator, 0)
Outside diameter	INTEG (resistance increment, 9.77e + 011)
Permeate flux	1
Pure water flux after backwashing	35 − STEP(35, 100)
Pure water flux after filtration	0 + STEP(46, 100)
Pure water membrane special flux	Table function of pure water flux after filtration(time)
Recovering length	54.06
Resistance increment	8 × outside diameter × backwashing flux × 1.46/1.5 × transport properties of backwashing/inside diameter^2/1,000
Table function of pure water flux after filtration	(Total resistance − membrane resistance)-STEP((total resistance − membrane resistance), 100) ([(0, 0) − (106, 60)], (0, 54.06), (10, 51), (20, 50), (30, 49), (40, 47), (50, 46), (60, 45), (70, 44), (80, 41), (90, 41), (100, 40), (106, 40))
Temperature	26.4
The backwash coefficient	0 + STEP(1/(total resistance × viscosity), 100)
TMP after backwashing	Backwashing flux × The backwash coefficient
TMP table function	([(0, 0) − (106, 400)], (0, 140), (10, 170), (20, 180), (30, 200), (40, 210), (50, 250), (60, 280), (70, 310), (80, 320), (90, 340), (100, 360), (106, 360))
Total resistance	Transmembrane pressure/permeate flux/viscosity
Transmembrane pressure	TMP table function(time)
Viscosity	0.001792/(1 + 0.00337 × temperature + 0.00221 × temperature^2)

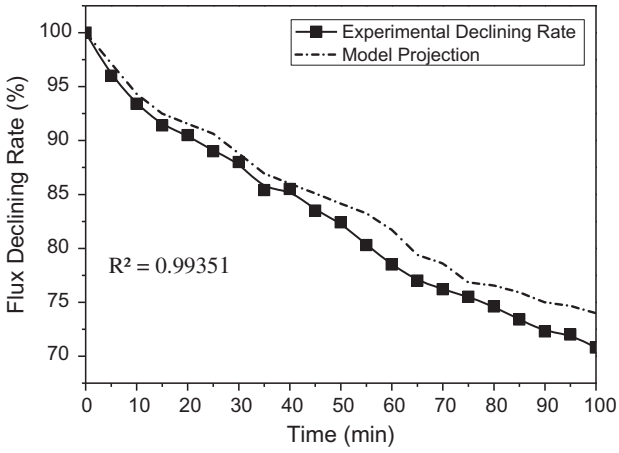

Fig. 7. Comparison of experimental data and model output for the flux declining rate.

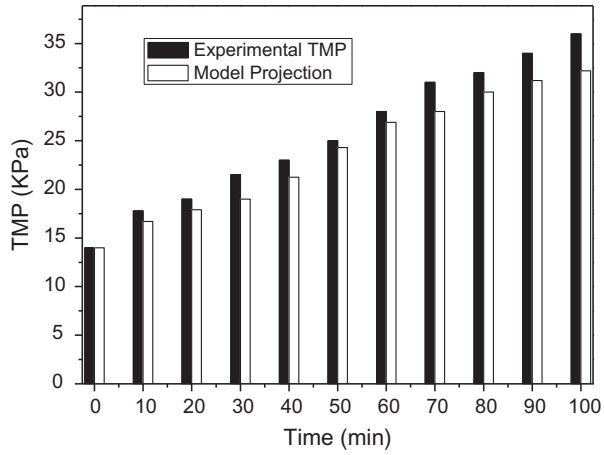

Fig. 8. Comparison of experimental TMP data and the model projection.

$$J_0 = \frac{\Delta P}{\mu(R_t)} = \frac{\Delta P}{\mu(R_m + R_c + R_a)} \quad (1)$$

where J_0 is the permeate flux, $m^3/(m^2\,h)$; ΔP is TMP, Pa; μ is the permeate viscosity, Pa s; R_t is the total resistance, m^{-1}; R_m is the intrinsic membrane resistance, m^{-1}; R_c is the cake layer resistance, m^{-1}; and R_a is the adsorption resistance, m^{-1}, which is typically due to adsorption of solutes and pore blocking. The increased portion of TMP was considered to be caused by R_c and R_a. R_c caused fouling which could be reversed by hydraulic cleaning, specifically backwashing. The membrane module was backwashed with permeate water for 5 min to remove the cake layer from the surface of the membrane. The remaining portion of TMP was regarded as the resistance caused by R_a. R_a caused irreversible fouling that could only be eliminated by chemical cleaning.

As shown in Fig. 9, the total resistance (R_t) increased continuously and rapidly, and exhibited a good linear relationship ($R^2 = 0.9946$) with operating

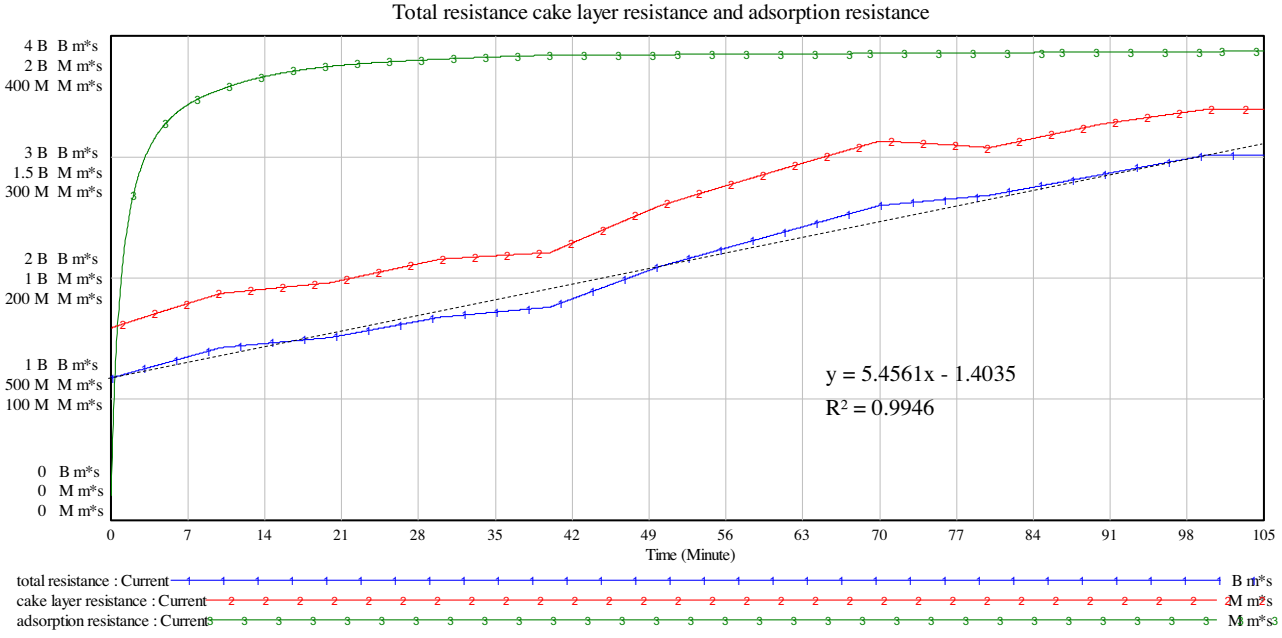

Fig. 9. Variation of R_t, R_c, and R_a in our SD model.

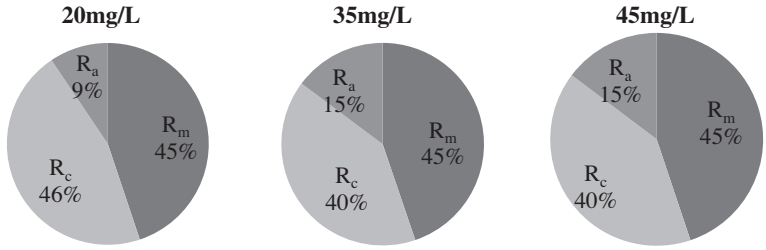

Fig. 10. Relative share of total resistance (R_t) made up by membrane resistance (R_m), cake resistance (R_c), and absorption resistance (R_a) of $FeCl_3$ of 20, 35, and 45 mg/L.

time throughout the entire time interval. The model projection curves of Fig. 9 show that the cake resistance (R_c) increased over time, after the addition of block copolymer, and after the addition of the surface cake layer. Change in adsorption resistance (R_a) indicated the transition from rapid initial fouling to slow long-term fouling took place during the first 20 min. In magnitude, R_a was a small component of R_t (≤15%). Despite the constant R_a from 20 min to nearly the end of the simulation, R_t exhibited an increasing trend due to the continuous increase in R_c, suggesting that R_c is the main cause of the increase in resistance.

Conclusions drawn from our SD model were consistent with prior practical filtration experiments [25,26]. Our analysis supports the conclusion that SD modeling can be used as a tool to estimate the resistance of coagulation–UF process system, even with limited experimental data of TMP and flux.

3.2.2. Composition of total resistance

The contribution of each type of resistance to membrane fouling was determined using the SD model. As shown in Fig. 10, a decrease in R_c was observed along with an increase in coagulant concentration ($FeCl_3$) from 20 to 35 mg/L, but total resistance decreased by 40% overall. R_a remained constant. R_c decreased from 46 to 40% of the total resistance. These results show that coagulation prevents suspended particles, colloid

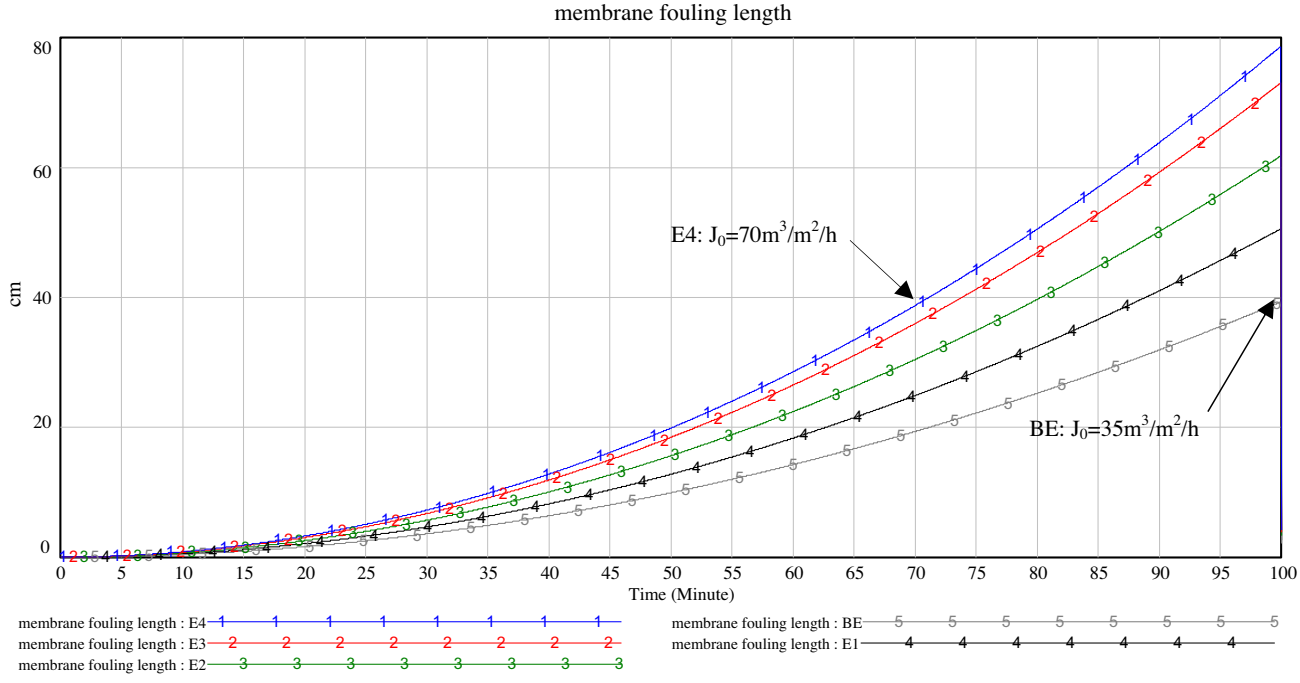

Fig. 11. Projections of membrane fouling length in the BE, experiment 1 (E1), experiment 2 (E2), experiment 3 (E3), and experiment 4 (E4).

formation, and part of the dissolution of organic matter, which can form strong bonds that contribute to R_c [27]. As the concentration of coagulant increased from 35 to 45 mg/L, no evidence of any sudden increase in membrane fouling was observed, and the relative contributions of the different resistances remained constant. This was likely due to a coagulant concentration sufficient to facilitate the formation of flocculation, which would not significantly impact R_c. In this manner, the SD model is a useful tool for minimizing coagulant concentration with regard to mitigating membrane fouling.

3.2.3. Dynamics of membrane fouling

In order to determine the relationship between membrane flux and the length of membrane fouling, the length of membrane fouling was simulated under different permeate flux conditions. The results are shown in Fig. 11. The initial permeate flux (J_0) was 35 $m^3/(m^2\ h)$ in a basic experiment (BE). It increased to 45 $m^3/(m^2\ h)$ in experiment 1 (E1), 55 $m^3/(m^2\ h)$ in experiment 2 (E2), 65 $m^3/(m^2\ h)$ in experiment 3 (E3), and 70 $m^3/(m^2\ h)$ in experiment 4 (E4). Fig. 11 clearly shows that different J_0 values led to different membrane fouling lengths. Low flux led to less membrane fouling than high flux. J_0 was kept constant for BE and E4. Other variable factors were also kept unaltered. Using these options, membrane fouling was projected to reach full length (40 cm) by 100 min in BE and 70 min in E4. The time required by membrane fouling in E4 was expected to be 70% that of BE, and its J_0 twice that of BE. In Fig. 11, the membrane fouling growth was visibly linked to J_0. In practice, J_0 could be one of the parameters employed to mitigate the level and growth of membrane fouling.

3.2.4. Relationship between the rate of membrane fouling and backwashing times

Based on the previous results and discussions, the role of coagulation was postulated to be a suitable means of interpreting the effects of coagulation on fouling. As the coagulated water filters, flocs deposit on the surface of the membrane, forming a loose, porous cake. The cake could be easily removed by backwashing, because it was not closely adhered to the surface [28]. This may mean that backwashing can completely protect the membrane from fouling, as is shown in Fig. 12, which shows experimental and modeling evidence. The results of the model were consistent with the experimental data.

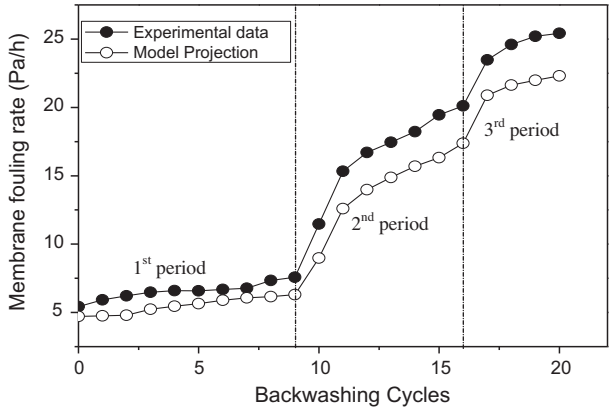

Fig. 12. Comparison of the experimental membrane fouling rate data with the model's projection.

Fig. 12 shows the cyclic nature of the filtration-backwashing process. The fouling rate climbed slowly during the first period. This suggests that the main type of membrane fouling was R_c during the initial filtration. Small suspended particles were deposited on the cake layer instead of on the membrane surface, allowing the recovery of flux after backwashing. As the number of filtration–backwashing cycles increased, the membrane fouling rate ascended significantly. After backwashing, the membrane fouling rate still became faster and faster in each filtration cycle during the second period. It was, therefore, concluded that the flux did not recover completely due to the substantial cake layer adhering to the surface of the membrane, and that this layer could not be easily removed by backwashing. In the third period, more and more small particles were adsorbed onto the cake layer and membrane pores, forming irreversible fouling. The membrane fouling rate increased gradually.

During the first period, the membrane was protected by the cake layer and fit to filtration. Even though fouling occurred, it was easily removed by backwashing. The membrane fouling rate rapidly increased during the second period. Backwashing was not sufficient when the membrane was fouled. During the third period, although physical washing could not restore membrane performance, chemical membrane cleaning was needed to recover the 16th time. This is shown in Fig. 12, which depicts results obtained by running the model. Fig. 12 also shows that the fouling rate was 22.5 Pa/h during the third period, nearly the four times that of the first period (5 Pa/h). As was previously discussed, when the model is used to simulate the coagulation–UF process, it is expected that the SD model will play an important role in

simulating the rate of membrane fouling and predicting membrane lifespan.

4. Conclusion

In this manuscript, we discussed attempts to understand dynamic behaviors in coagulation–UF processes via SD analysis through the prediction of experimental data. This culminated in several key results:

(1) A SD model for the coagulation–UF system was developed. The model was used to provide a convenient and visual way of evaluating and making projections of coagulation–UF process.
(2) Absorption resistance was projected to contribute a small part of total resistance (≤15%) in the BE. Permeate flux was 35 $m^3/(m^2\ h)$, and the concentration of coagulant was 35 mg/L. Cake resistance was identified as the main cause of the increase in resistance. It was analyzed using the model.
(3) The composition of total resistance to membrane fouling was obtained using the SD model. As the concentration of coagulant increased from 20 to 35 mg/L, total resistance decreased by 40% and cake resistance decreased from 46 to 40% of the total resistance, suggesting that the concentration of coagulant and the removal rate of membrane fouling were positively correlated. As the concentration of coagulant increased from 35 to 45 mg/L, there was no obvious impact on resistance, suggesting that the concentration of coagulant was sufficient at 35 mg/L. As indicated by analysis of the SD model, it was easy to minimize coagulant concentration to mitigating membrane fouling under different conditions.
(4) The simulation of the membrane fouling length under different permeate flux conditions (J_0) (35–70 $m^3/(m^2\ h)$) indicated that specifying an optimal J_0 could be one of the options for mitigating the level and growth of membrane fouling.
(5) As shown in Fig. 9, the rate of membrane fouling was found to be affected by backwashing times in the SD model. Membrane fouling was accelerated by increased adsorption resistance from the 2nd period. The model was designed to predict membrane lifespan and the time point of chemical cleaning (the 16th time in BE).

Ultimately, this study demonstrates that SD modeling can provide an efficient means of optimizing the coagulation–UF process of drinking water treatment, and that these models can be also applied to process optimization in other areas of water treatment.

Acknowledgments

This research project was supported by the National Science Foundation, China (project reference No.: 51308390) and the key project of the National Social Science Foundation, China (project reference No.: 13AZD011): The development of city water and river basin water ecological environment protection.

References

[1] A. Affandy, E. Keshavarz-Moore, H.K. Versteeg, Application of filtration blocking models to describe fouling and transmission of large plasmids DNA in sterile filtration, J. Membr. Sci. 437 (2013) 150–159.
[2] W. Gao, H. Liang, J. Ma, M. Han, Z.L. Chen, Z.S. Han, G.B. Li, Membrane fouling control in ultrafiltration technology for drinking water production: A review, Desalination 272 (2011) 1–8.
[3] J. Colomer, F. Peters, C. Marrasé, Experimental analysis of coagulation of particles under low-shear flow, Water Res. 39 (2005) 2994–3000.
[4] J.L. Lin, C.P. Huang, C.J.M. Chin, J.R. Pan, Coagulation dynamics of fractal flocs induced by enmeshment and electrostatic patch mechanisms, Water Res. 42 (2008) 4457–4466.
[5] E. Barbot, S. Moustier, J.Y. Bottero, P. Moulin, Coagulation and ultrafiltration: Understanding of the key parameters of the hybrid process, J. Membr. Sci. 325 (2008) 520–527.
[6] C. Staaks, R. Fabris, T. Lowe, C.W.K. Chow, J.A. van Leeuwen, M. Drikas, Coagulation assessment and optimisation with a photometric dispersion analyser and organic characterisation for natural organic matter removal performance, Chem. Eng. 168 (2011) 629–634.
[7] B. Cancino-Madariaga, R. Ruby, C.A. Castro, J.S. Torrico, M.L. Riquelme, Analysis of the membrane fouling mechanisms involved in clarified grape juice ultrafiltration using statistical tools, Ind. Eng. Chem. Res. 51 (2012) 4017–4024.
[8] A. Abdelrasoul, H. Doan, A. Lohi, A mechanistic model for ultrafiltration membrane fouling by latex, J. Membr. Sci. 433 (2013) 88–99.
[9] K. Masoudnia, A. Raisi, A. Aroujalian, M. Fathizadeh, Treatment of oily wastewaters using the microfiltration process: Effect of operating parameters and membrane fouling study, Sep. Sci. Technol. 48 (2013) 1544–1555.
[10] E.V. Tsagaraki, H.N. Lazarides, Fouling analysis and performance of tubular ultrafiltration on pretreated olive mill waste water, Food Bioprocess Technol. 5 (2012) 584–592.
[11] K. Vizayakumar, P.K.J. Mohapatra, Environmental impact analysis of a coalfield, J. Environ. Manage. 34 (1991) 73–93.

[12] K. Vizayakumar, P.K.J. Mohapatra, Modelling and simulation of environmental impacts of coalfield: System dynamics approach, J. Environ. Syst. 22 (1993) 59–73.
[13] J. Caiado, Performance of combined double seasonal univariate time series models for forecasting water demand, J. Hydrol. Eng. 15 (2010) 215–222.
[14] M.S. Babel, A. Das Gupta, P. Pradhan, A multivariate econometric approach for domestic water demand modeling: An application to Kathmandu, Nepal, Water Resour. Manage. 21 (2007) 573–589.
[15] C. Guigui, J.C. Rouch, L. Durand-Bourlier, V. Bonnelye, P. Aptel, Impact of coagulation conditions on the in-line coagulation/UF process for drinking water production, Desalination 147 (2002) 95–100.
[16] Y. Wang, Y.B. Chu, B.-Y. Gao, Q.Y. Yue, W.Z. Zhou, On-line optical determination of floc by using an optical monitor, J. Harbin Inst. Technol. 12(New Series) (2005) 62–68.
[17] H. Bai, G.B. Li, Fuzzy based auto-coagulation control through photometric dispersion analyzer, J. Harbin Inst. Technol. 11(New Series) (2004) 164–167.
[18] Y.K. Lee, Y.J. Won, J.H. Yoo, K.H. Ahn, C.H. Lee, Flow analysis and fouling on the patterned membrane surface, J. Membr. Sci. 427 (2013) 320–325.
[19] K.A. Stave, A system dynamics model to facilitate public understanding of water management options in Las Vegas, Nevada, J. Environ. Manage. 67 (2003) 303–313.
[20] S. Anand, P. Vrat, R.P. Dahiya, Application of a system dynamics approach for assessment and mitigation of CO_2 emissions from the cement industry, J. Environ. Manage. 79 (2006) 383–398.
[21] S. Anand, R.P. Dahiya, V. Talyan, Investigations of methane emissions from rice cultivation in Indian context, Environ. Int. 31 (2005) 469–482.
[22] Ventana Systems, Inc., Vensim PLE software version 3.0, Ventana Systems, Inc., Harvard, MA, 1998.
[23] S. Judd, The status of membrane bioreactor technology, Trends Biotechnol. 26 (2008) 109–116.
[24] D. Jang, Y. Hwang, H. Shin, W. Lee, Effects of salinity on the characteristics of biomass and membrane fouling in membrane bioreactors, Bioresour. Technol. 141 (2013) 50–56.
[25] Y.F. Zhao, L.P. Zhu, Z. Yi, B.K. Zhu, Improving the hydrophilicity and fouling-resistance of polysulfone ultrafiltration membranes via surface zwitterionicalization mediated by polysulfone-based triblock copolymer additive, J. Membr. Sci. 440 (2013) 40–47.
[26] W.S. Guo, H.H. Ngo, J.X. Li, A mini-review on membrane fouling, Bioresour. Technol. 122 (2012) 27–34.
[27] C. Musikavong, S. Wattanachira, Identification of dissolved organic matter in raw water supply from reservoirs and canals as precursors to trihalomethanes formation, J. Environ. Sci. Health., Part A 48 (2013) 760–771.
[28] J.D. Lee, S.H. Lee, M.H. Jo, P.K. Park, C.H. Lee, J.W. Kwak, Effect of coagulation conditions on membrane filtration characteristics in coagulation−microfiltration process for water treatment, Environ. Sci. Technol. 34 (2000) 3780–3788.